

FWI IMAGING WITH SIMULTANEOUS ANISOTROPY ESTIMATION

J. McLeman¹, T. Burgess¹, T. Rayment¹

¹ DUG Technology

Summary

Full waveform inversion (FWI) can use reflections and refractions to generate not only high-resolution velocity updates but detailed intercept-reflectivity volumes as well. However, assuming kinematic errors in the supplied models are solely due to errors in velocity will result in incorrect estimations of the updated velocity and incorrect depth positioning of migrated events. Correct estimation of these requires a sufficiently accurate knowledge of anisotropy fields obtained by other means prior to running FWI. It would therefore be beneficial to jointly update velocity and anisotropy during a model building workflow with multi-parameter FWI. We demonstrate a novel simultaneous three-parameter FWI for velocity, epsilon and intercept-reflectivity using both reflections and refractions. The FWI kernel is decomposed to form the imaged intercept-reflectivity while the tomographic components of the diving waves and reflections are used to constrain the vertical and horizontal kinematics. To ensure correct primary amplitudes and use of multiple energy in the inverted intercept-reflectivity, a robust source-wavelet inversion is essential. Common multi-parameter inversion challenges are addressed using a sophisticated second-order quasi-Newton optimizer and inversion preconditioners. This new approach is demonstrated using a dataset from the Australian North-West Shelf.

FWI imaging with simultaneous anisotropy estimation

Introduction

Conventionally, full waveform inversion (FWI) uses diving waves to invert for P-wave velocity (V_p) while holding other subsurface parameters constant. This necessitates that the non-inverted parameters are sufficiently correct otherwise any error in the kinematics due to, for example, anisotropic parameters, will be incorrectly attributed to an error in V_p . As a result, the inverted velocity may produce depth errors and residual move-out on the image gathers. Consequently, it is preferable to jointly update V_p and anisotropy during a model building workflow with a multi-parameter FWI.

Performing multi-parameter FWI is, however, non-trivial. Large relative scale differences between the inverted parameters will result in notably slower convergence for the weaker parameter. There is also crosstalk between coupled inverted parameters where an error in one parameter is wrongly attributed to an error in the other (Operto et al., 2013). Sophisticated second-order optimisation strategies and preconditioners are required to address these issues adequately and efficiently. In this paper, we assume that delta has been robustly determined by other means (for example, through well calibration).

The joint inversion of V_p and epsilon is poorly constrained when using only diving waves. Such waves dominantly travel at the horizontal velocity which is a combination of the vertical velocity and epsilon. Therefore, errors in one or both parameters cannot be decoupled. The inclusion of reflections, which have more vertical travel paths, is required to reduce the non-uniqueness of solutions caused by the coupling of the two parameters (Cheng et al., 2016).

Including both reflections and refractions in FWI presents further challenges (Yao et al., 2020). Modelling data with smooth model parameters will produce only diving waves and the direct arrival. If the input data to FWI contains both reflections and diving waves, then the initial gradient will contain contributions from the higher-wavenumber “migration” term and the limited penetration depth “banana” term respectively. The migration term will have an amplitude proportional to the reflection coefficient, R , and represents the imaged result. Later iterations use the migration term to scatter the wavefield and additionally create the lower wavenumber reflection tomographic updates (“rabbit ears”) which control the kinematics and have an amplitude proportional to R^2 . The “migration” term and typically also the “banana” term will be preferentially inverted due to their higher amplitude. Without special care, the vertical velocity constraint (“rabbit ears”) will not significantly contribute to the inversion.

To overcome these challenges, this paper demonstrates a three-parameter multi-scattering FWI approach that uses reflections and refractions. This method simultaneously inverts for velocity, epsilon and intercept-reflectivity using an augmented wave equation approach and a novel second-order quasi-Newton optimiser with crosstalk mitigation (McLeman et al., 2021). We show real data examples of this approach from the North-West Shelf region of Western Australia.

Method

Using a dual-source towed streamer dataset with 8 cables and 6 km offsets located in the Australian NW continental shelf, a set of higher-resolution models for V_p , epsilon and intercept-reflectivity were built with visco-acoustic TTI FWI using the augmented wave equation. The initial V_p and anisotropy were obtained from existing regional models. Wells located inside the survey were used to refine delta. FWI was then run from 4 Hz to 8 Hz using a diving wave, V_p only inversion. At 12 Hz, both diving waves and reflections were included and the simultaneous three-parameter visco-acoustic FWI was performed.

A key component to the success of the three-parameter inversion was the adequate estimation of the source wavelet. Using near-field hydrophones (NFH) (Ziolkowski et al., 1982) or gun array modelling to determine source signatures will not ensure an amplitude match between the modelled and observed data in FWI since they will differ by at least a scale factor. These amplitude discrepancies are often mitigated by using kinematic only objective functions (Warner et al., 2013). However, both the

kinematics and dynamics are required when estimating intercept-reflectivity with FWI. An incorrect source wavelet amplitude will yield incorrect estimations of primary reflection amplitudes and sub-optimal use and attenuation of multiples during FWI imaging. Since NFH data were not available, a gun-array modelled signature was obtained and then refined by a shot-by-shot source wavelet inversion prior to FWI (Virieux and Operto, 2009). The source wavelet inversion used least-squares matching on the direct arrival of the modelled and observed data to determine a robust true amplitude source wavelet.

The FWI gradient was decomposed into separate tomographic and migration terms using non-stationary filters discriminating on scattering angle in the wavenumber domain. The migration term generated the FWI intercept-reflectivity image, and the “banana” and “rabbit ears” tomographic terms updated epsilon and velocity. Epsilon was further refined during the inversion with structurally oriented smoothing (Fehmers and Höcker, 2003). Crosstalk, as well as relative scaling differences between model points and inverted parameters were addressed using a novel AdaGrad + L-BFGS optimiser which has shown significant convergence improvements over conventional L-BFGS (McLeman et al., 2021).

Results

The initial and updated velocity models overlain on their respective Kirchhoff preSDM stacks are given by Figures 1a) & d). The corresponding initial and updated epsilon models are shown in Figures 1b) & e). The updated velocity and anisotropy models show a clear geological conformance. The horizon depth compared with a well marker for the initial models is shown in Figure 1c), the well-tie improvements brought by the simultaneous inversion are shown in Figure 1f).

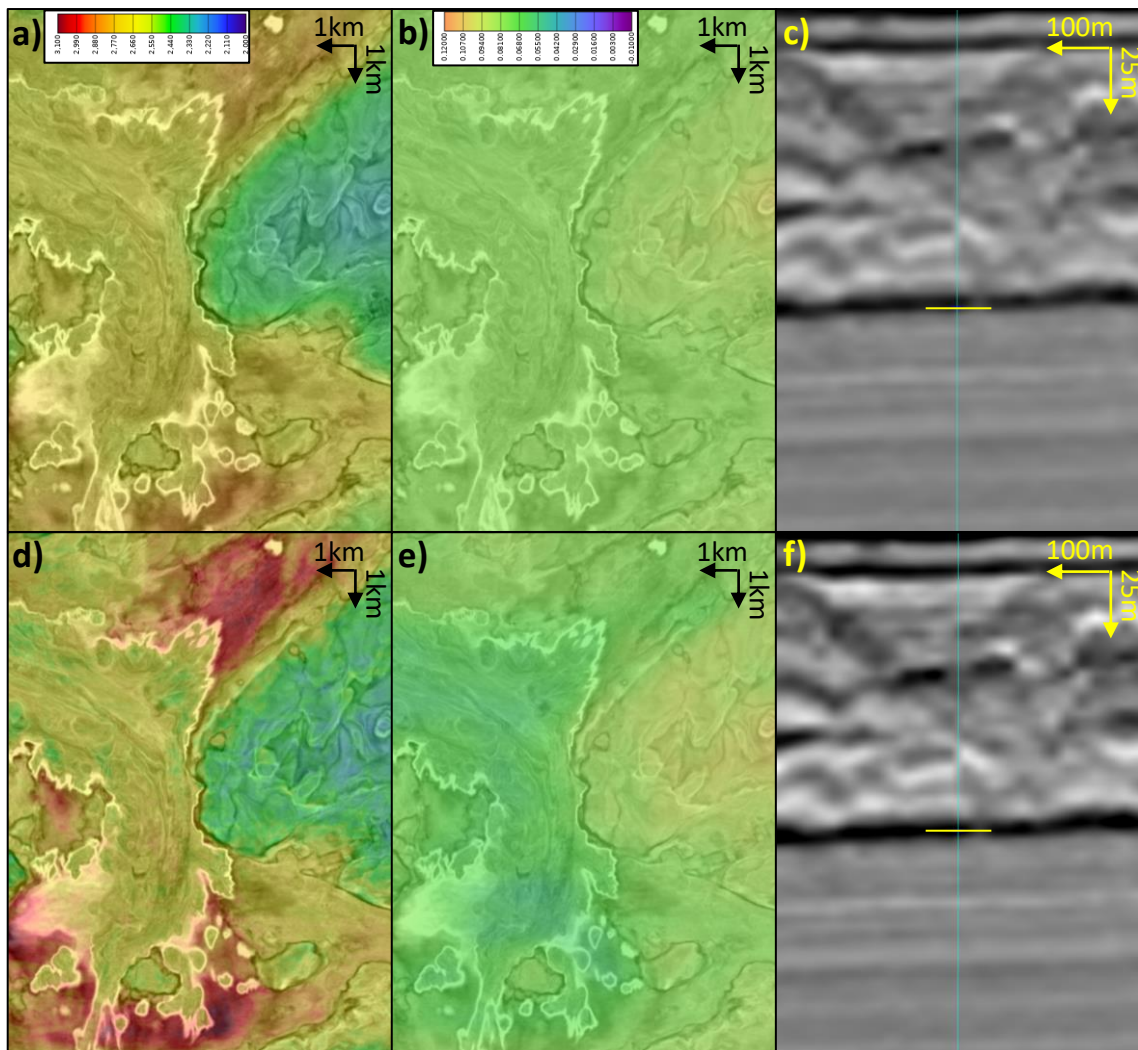


Figure 1 Kirchhoff preSDM stacks with initial velocity and epsilon models overlaid a), b) and the updated models d), e). Horizon and well marker for initial models c) and updated models f).

Figures 2a), b) & c) show Kirchhoff migrated common image gathers and a 0-40 degree angle stack with the models input to the 12 Hz three-parameter FWI. Figures 2d), e) & f) show Kirchhoff migrated results using the updated velocity and epsilon models. An improvement in gather flatness is observed even at high angles due to the improved anisotropy estimation. The updated models have yielded a clear improvement in structural simplicity and focusing throughout the section.

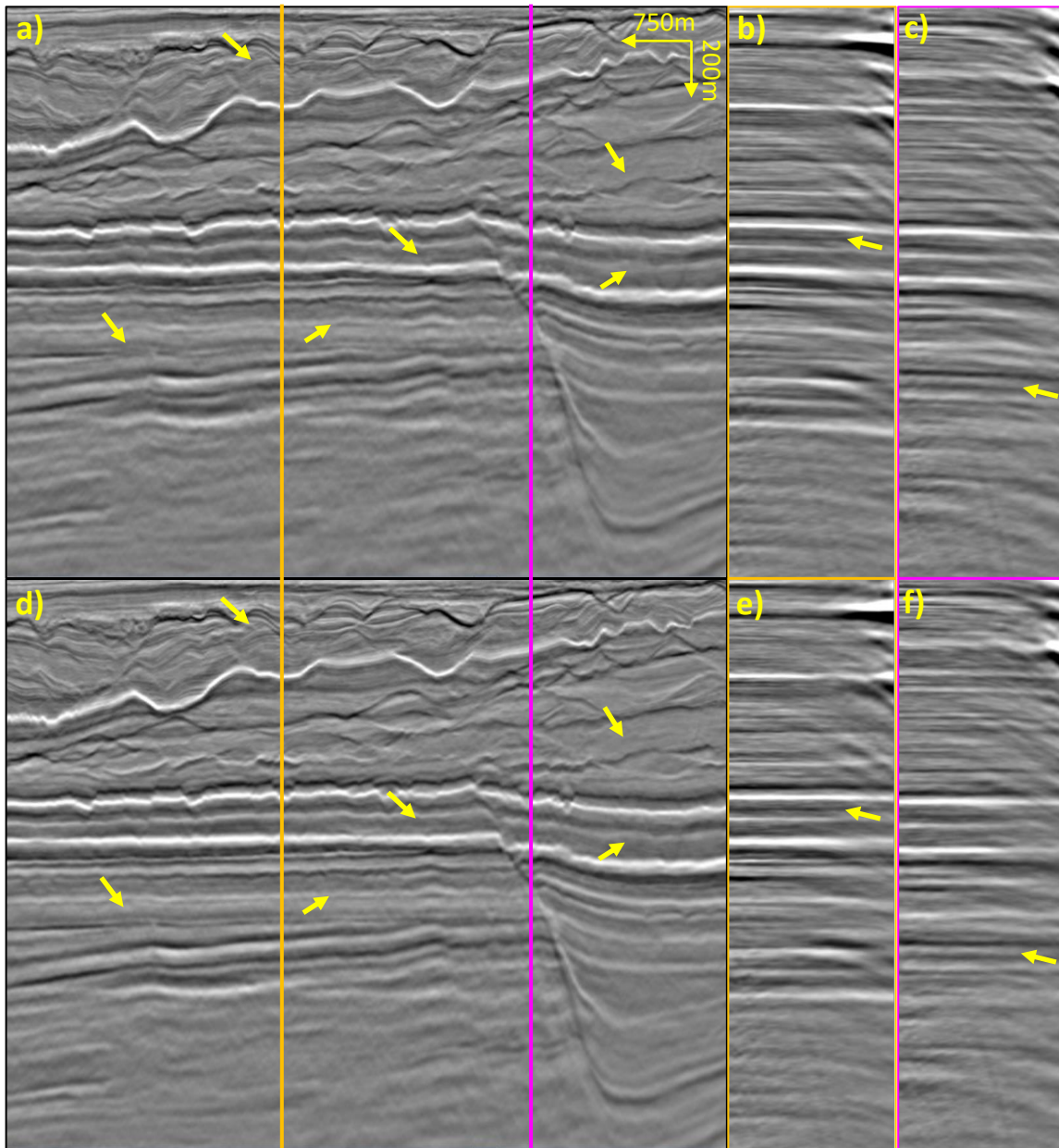


Figure 2 3D preSDM Kirchhoff migrations, a) 0-40 deg angle stack with the input models, b), c) are image gathers using the input models, d) 0-40 deg angle stack with the updated velocity and epsilon models, e), f) are image gathers using the updated models.

Figures 3a) & b) show a depth slice at 1340 m of a Kirchhoff preSDM stack with the updated velocity and epsilon (3a) and the FWI inverted intercept-reflectivity (3b). The Kirchhoff stack was filtered to the inversion frequency of the FWI image for a fair comparison. A conventional workflow using all available shots provided the input to the Kirchhoff migration. The inverted intercept-reflectivity used only 1/3 of the unprocessed shots as input. Although there is a good amplitude and structural similarity between the two images, the FWI image shows an improvement in resolution and better event delineation. To generate this FWI image, FWI has used the primaries, multiples and ghosts to perform model building and least-squares imaging simultaneously.

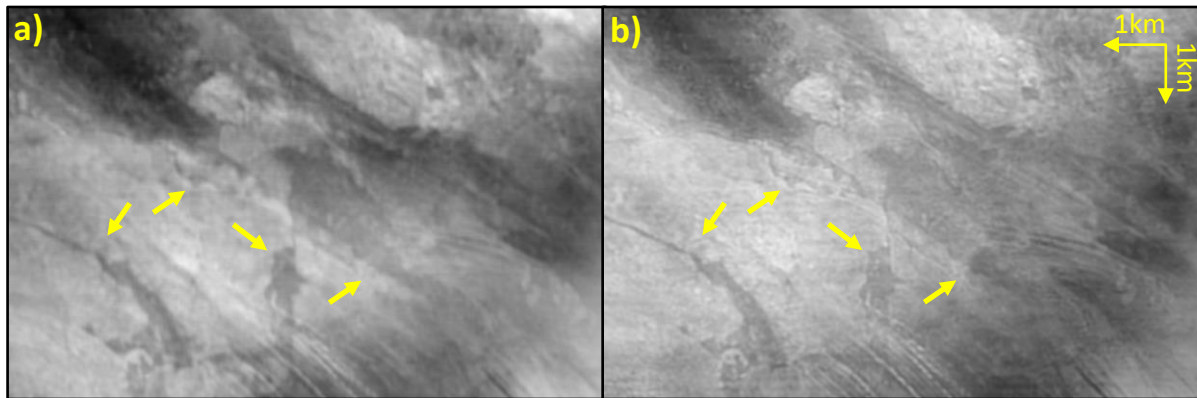


Figure 3 A depth slice at 1340 m of a) the Kirchhoff 3D preSDM using the updated velocity and epsilon, and b) the intercept-reflectivity generated by FWI.

Conclusions

We have shown an FWI model building and imaging technique which determines velocity, epsilon and intercept-reflectivity simultaneously in a three-parameter inversion using raw field data as input. Even though only 1/3 of the unprocessed shots were used in the inversion, the intercept-reflectivity compares very favourably against the Kirchhoff migration that had undergone a full processing sequence using all the shots. FWI has used the primaries, multiples and ghosts to perform model building and least-squares imaging. Prior to running FWI, an inversion was used to refine the initial modelled signature into a true amplitude source wavelet to ensure that the intercept-reflectivity amplitudes were accurate. The inclusion of epsilon in the inversion achieved improved mis-ties with known well-markers. Common challenges of multi-parameter inversions that include reflections were addressed using a sophisticated second-order quasi-Newton optimisation scheme and inversion preconditioners.

Acknowledgements

We would like to thank Multi-Client Resources (MCR) for permission to use the BEX MC3D real dataset example and DUG Technology (DUG) for allowing us to present this work.

References

- Cheng, X., Jiao, K., Sun, D. and Vigh, D. [2016]. Multiparameter estimation with acoustic vertical transverse isotropic full-waveform inversion of surface seismic data, *Interpretation*, **4**, SU1-SU16.
- Fehmers, G. C. and Höcker, C. F. W. [2003]. Fast structural interpretations with structure-oriented filters, *Geophysics*, **68**(4), 1286-1293.
- McLeman, J., Burgess, T., Sinha, M., Hampson, G. and Thompson, T. [2021]. Reflection FWI with an augmented wave equation and quasi-Newton adaptive gradient scheme, *First International Meeting for Applied Geoscience & Energy*, Expanded Abstracts, 667-671.
- Operto, S., Gholami, Y., Prioux, V., Ribodetti, A., Brossier, R., Metivier, L. and Virieux, J. [2013]. A guided tour of multiparameter full-waveform inversion with multicomponent data: From theory to practice, *The Leading Edge*, **32**(9), 1040-1054.
- Virieux, J. and Operto, S. [2009]. An overview of full-waveform inversion in exploration geophysics, *Geophysics*, **74**(6), WCC1-WCC26.
- Warner, M., Ratcliffe, A., Nangoo, T., Morgan, J., Umpleby, A., Shah, N., Vinje, V., Štekl, I., Guasch, L., Win, C., Conroy, G., and Bertrand, A. [2013]. Anisotropic 3D full-waveform inversion, *Geophysics*, **78**(2), R59-R80.
- Yao, G., Wu, D. and Wang, S. X. [2020]. A review on reflection-waveform inversion, *Petroleum Science*, **17**, 334-351.
- Ziolkowski, A., Parkes, G., Hatton, L. and Haugland, T. [1982]. The signature of an air gun array: Computation from near-field measurements including interactions, *Geophysics*, **47**(10), 1413-1421.